# RNA and the Goldilocks Zone: Where $Mg^{2+}$ concentration is just right

Rebecca Guth-Metzler[1,2], Ahmad Mohyeldin Mohamed[1,2,3], Elizabeth T. Cowan[1], Moran Frankel-Pinter[1,2,3], Roger M. Wartell[1,2,4], Jennifer B. Glass[2,5,6], and Loren Dean Williams[1,2,3,5*].

[1]School of Chemistry and Biochemistry, Georgia Institute of Technology, Atlanta, GA, USA, 30332
[2]NASA Center for the Origin of Life, Georgia Institute of Technology, Atlanta, GA, USA, 30332
[3]NSF/NASA Center for Chemical Evolution, Atlanta, GA, USA
[4]School of Biological Sciences, Georgia Institute of Technology, Atlanta, GA 30332
[5]Petit Institute of Bioengineering and Bioscience, Georgia Institute of Technology, Atlanta, GA, USA, 30332
[6]School of Earth and Atmospheric Sciences, Georgia Institute of Technology, Atlanta, GA, USA, 30332.

*Loren Dean Williams.

**Email:** Loren.Williams@chemistry.gatech.edu

**Competing Interest Statement:** The authors have no competing interests.

**This PDF file includes:**

Main Text
Figures 1 to 5
Table 1

## Abstract

$Mg^{2+}$, the most abundant divalent cation in cells, catalyzes RNA cleavage but can also promote RNA folding. Because folding can protect RNA from cleavage, we predicted a "Goldilocks zone", which is a local maximum in RNA lifetime at the minimum $Mg^{2+}$ concentration required for folding. By simulation and experiment, we characterized the RNA Goldilocks zone and its dependence on cleavage parameters and extent of folding. We show experimentally that yeast $tRNA^{Phe}$ can inhabit a Goldilocks zone. The Goldilocks phenomena appears to be robust and is tunable by changes in magnesium affinity, and a variety of other factors. Goldilocks behavior can be more pronounced for RNAs with intermediate folding states. Goldilocks behavior allows ultrafine control of RNA chemical lifetime. A subset of RNAs *in vivo* are expected to occupy the Goldilocks zone. In evolutionary context, Goldilocks behavior may have shaped RNA in an early Earth environment containing $Mg^{2+}$ and other metals. RNAs that do not fold cannot access a Goldilocks zone.

## Significance Statement

RNA, nature's most fragile biopolymer, can inhabit a "Goldilocks zone" of chemical protection. Using simulation and experiment, we show that in the Goldilocks zone, RNA is protected by $Mg^{2+}$ contributions to RNA folding, offsetting contributions to cleavage. RNA is shifted in and out of the Goldilocks zone by changes in $[Mg^{2+}]$ and by other factors. The effects of cation concentrations, temperature, RNA sequence, and chemical modification on Goldilocks behavior allow ultrafine control of RNA chemical lifetime. The RNA Goldilocks zone may have played a role in the emergence of RNA during prebiotic chemical processes.

## Introduction

Universal biopolymers (DNA, RNA, protein, and carbohydrate) are ephemeral (1). Biopolymers hydrolyze in aqueous media, degrading to the level of monomers. In aqueous solution, hydrolysis of biopolymers is always thermodynamically favored. However, very low rates of hydrolysis, due to kinetic trapping, allow biopolymers to persist for extended periods of time.

RNA is especially fragile. In-line attack by 2'OH groups on adjacent phosphates catalyzes RNA cleavage (2-4) in reactions accelerated by divalent cations (5-8). However, divalent cations also promote folding of RNAs (9-13), and are generally required for catalytic function of ribozymes (14-16), and for RNA biosynthesis (17), and RNA processing by protein enzymes (18). $Mg^{2+}$, the most abundant divalent cation in cells (19), is dangerous to RNA but is required for RNA function.

Here we show that RNA can inhabit a "Goldilocks zone" in which RNA lifetime is locally maximized. A Goldilocks zone of RNA protection is flanked by conditions of fragility. RNA is shifted in and out of the Goldilocks zone by changes in $[Mg^{2+}]$ and other by factors, in either direction. Using simulation and experiment, we show that in the Goldilocks zone, RNA is protected by $Mg^{2+}$ contributions to RNA folding, offsetting $Mg^{2+}$ contributions to cleavage.

We hypothesized an RNA Goldilocks zone because a general increase in $Mg^{2+}$-catalyzed cleavage might be balanced by a decrease in cleavage due to $Mg^{2+}$-facilitated folding (5, 20). In fact, attenuation of RNA cleavage is a useful experimental marker for RNA folding (2, 21-25). Folding

protects RNA from degradation by converting floppy RNA into structured RNA, which is less likely to adopt the geometry required for cleavage. RNA folding increases the depths of kinetic traps.

Our simulations incorporate the influence of $Mg^{2+}$ on both folding and cleavage of RNA. The simulations show RNA Goldilocks behavior over a broad range of $Mg^{2+}$ dependencies, rates of cleavage, and folding models. Experiments confirmed the simulation results; yeast $tRNA^{Phe}$, a model system for studying RNA (26, 27), has a Goldilocks zone. A local maximum lifetime of yeast $tRNA^{Phe}$ occurs at the $Mg^{2+}$ concentration where RNA is ~90% folded. By contrast, a control RNA that does not fold, $rU_{20}$ (polyuridylic acid 20-mer), does not display Goldilocks behavior. RNAs that do not fold do not show Goldilocks behavior. To our knowledge, simultaneous contributions of opposing forces to RNA lifetime have not previously been characterized or quantified.

## Results

*RNA lifetime responds to changes in [$Mg^{2+}$].* To characterize effects of $Mg^{2+}$ concentration (hereafter [$Mg^{2+}$]) on RNA lifetime, we schematically expressed relationships between [$Mg^{2+}$], RNA folding, and rates of RNA cleavage. Persistence is quantified as the RNA lifetime, which is the reciprocal of the pseudo-first order rate constant for cleavage. In our schema **(Figure 1),** a positive connection (+) between two parameters indicates a positive correlation. A negative connection (-) indicates a negative correlation. Increasing $Mg^{2+}$ can (i) increase the rate of RNA cleavage (5), and (ii) increase extent of RNA folding (28). Increased folding decreases rates of cleavage (2, 21-23). In sum, the effects of $Mg^{2+}$ on RNA persistence are expected to be pleomorphic, both protecting and degrading RNA. Folding is typically fast (28-32) compared to $Mg^{2+}$-catalyzed cleavage (3, 5, 6), so cleavage operates over a fixed fold landscape.

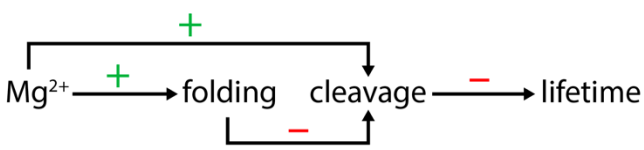


**Figure 1: Correlations of $Mg^{2+}$ effects on RNA**. Increasing [$Mg^{2+}$] tends to increase rates of cleavage. However, increased [$Mg^{2+}$] can increase the extent of folding, which reduces rate of cleavage. Pleomorphic RNA responses to $Mg^{2+}$ can cause Goldilocks behavior.

The relationships of **Figure 1** were converted into mathematical models that predict lifetimes of RNAs. The models describe both $Mg^{2+}$-driven cleavage and $Mg^{2+}$-driven protection via folding. A simple model assumes two states and more complex models allow folding intermediates. We used the Hill equation to describe extent of folding (33), although any model that reasonably describes RNA folding can be used. We assume that folding is faster than cleavage.

For a two-state model, the fraction folded is $f_f$ and the fraction unfolded is $f_u$ **(Eq. 1a and 1b)**:

$$\boldsymbol{f_f = \frac{1}{1 + \left(\frac{K_D}{[Mg^{2+}]}\right)^n}} \qquad \textbf{Eq. 1a}$$

$$\boldsymbol{f_f + f_u = 1} \qquad \textbf{Eq. 1b}$$

$K_D$ is the $[Mg^{2+}]$ at the folding midpoint (13) and n is the Hill coefficient, which reflects the cooperativity of RNA folding.

The effects of $Mg^{2+}$ on RNA cleavage are a second order phenomena in which the rate of cleavage depends on [RNA] and $[Mg^{2+}]$ (5, 6). The observed pseudo-first order rate constant ($k_{obs}$) is proportional to the second-order rate constant (k) and $[Mg^{2+}]$ **(Eq. 2)** (34):

$$\boldsymbol{k_{obs} = k[Mg^{2+}]} \qquad \textbf{Eq. 2}$$

To model RNA lifetime with a two-state folding model, we used two cleavage rate constants: $k_f$ for folded RNA and $k_u$ for unfolded RNA. Folding offers protection from cleavage, and therefore $k_f < k_u$. For an RNA that can occupy two states, $k_{obs}$ is a convolution of cleavage contributions based on fractional occupancies and rate constants for each state **(Eq. 3**, which is an extension of **Eq. 2** with differential cleavage based on folding):

$$\boldsymbol{k_{obs} = f_f k_f[Mg^{2+}] + f_u k_u[Mg^{2+}]} \qquad \textbf{Eq. 3}$$

RNA lifetime is the reciprocal of the observed cleavage rate constant ($k_{obs}$) **(Eq. 4)** (35):

$$\boldsymbol{lifetime = (k_{obs})^{-1} = \left( \frac{k_f[Mg^{2+}]}{1 + \left(\frac{K_D}{[Mg^{2+}]}\right)^n} + \left[ 1 - \frac{1}{1 + \left(\frac{K_D}{[Mg^{2+}]}\right)^n} \right] k_u[Mg^{2+}] \right)^{-1}} \qquad \textbf{Eq. 4}$$

*Simulations demonstrate Goldilocks behavior:* Using the mathematical scheme with two states we investigated the Goldilocks zone through simulations. Estimates of initial folding parameters, $K_D$ = 0.022 mM $Mg^{2+}$ and n = 4.1, were obtained from previous work (10). Initial estimates of relative rate constants were $k_u = 1\ t_{rel}^{-1}[Mg^{2+}]_{rel}^{-1}$ and $k_f = 0.2\ t_{rel}^{-1}[Mg^{2+}]_{rel}^{-1}$, consistent with changes in RNA cleavage rates upon conversion of single strands to duplex (36, 37).

The initial input parameters, entered into **Eq. 4**, reveal the general features of Goldilocks behavior **(Figure 2a)**. RNA that folds in response to $Mg^{2+}$ (solid line) shifts from a greater cleavage rate constant at lower $[Mg^{2+}]$ ($k = 1\ t_{rel}^{-1}[Mg^{2+}]_{rel}^{-1}$, dashed line) to a smaller cleavage rate constant at higher $[Mg^{2+}]$ ($k = 0.2\ t_{rel}^{-1}[Mg^{2+}]_{rel}^{-1}$, dotted line). The Goldilocks zone is where both behaviors contribute. From the apex of the Goldilocks zone, RNA lifetime decreases if $[Mg^{2+}]$ is either increased or decreased.

Goldilocks behavior is robust and present over a broad range of folding and cleavage parameters. Systematic changes in $K_D$, n, $k_u$, and $k_f$ in the simulations reveal the effects of each parameter **(Figure 2b-e)**. $K_D$ modulates the position of the Goldilocks zone on the $[Mg^{2+}]$ axis. RNAs that fold at lower $[Mg^{2+}]$ show a Goldilocks zone at lower $[Mg^{2+}]$. The Hill constant n modulates the sharpness of the Goldilocks peak without substantial change in position; a larger n gives a sharper peak. The parameters $k_u$ and $k_f$ modulate the slopes leading to and from the zone ($k_u$ modulates the left and $k_f$ modulates the right). The $k_u/k_f$ ratio modulates the amplitude of the peak. The simulations reveal special conditions under which the Goldilocks zone is absent (e.g. **Figure 2a**; dotted and dashed lines). These conditions are for RNAs that (i) do not fold, (ii) are always folded, (iii) lack a reduction in cleavage rate constant upon folding, or (iv) transition very gradually between differential cleavage realms with varying $[Mg^{2+}]$ **(Supp. Figure 1)**.

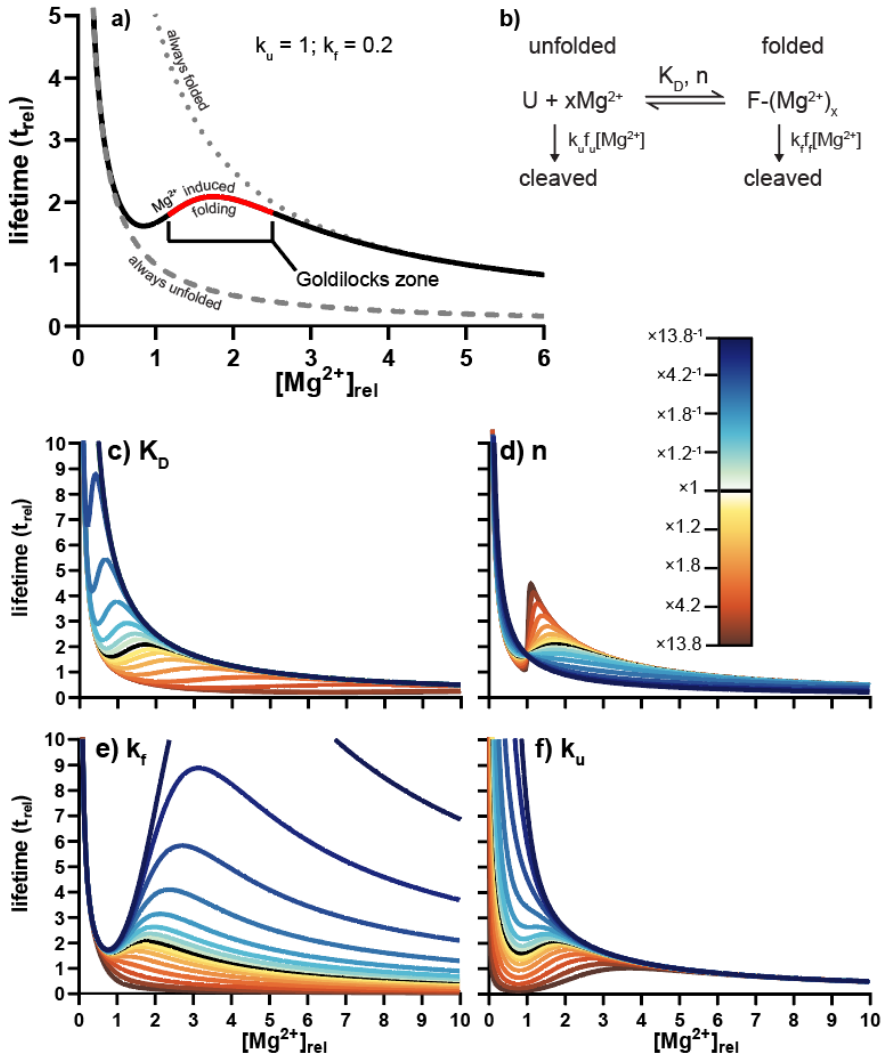


**Figure 2: Robust Goldilocks behavior of RNA is predicted by simulations.** (a) Simulations reveal the influence of $[Mg^{2+}]$ on the lifetime of an RNA that is cleaved more slowly in the folded state than in the unfolded state (black/red line). The Goldilocks zone is highlighted in red. The lifetime of an RNA that does not fold is shown by a dashed line (larger rate constant). The lifetime of an RNA that is always folded is shown by a dotted line (smaller rate constant). The folding RNA tracks the RNA with a large rate constant at low $Mg^{2+}$ and tracks the RNA with small rate constant at high $Mg^{2+}$. These simulations used $K_D$ = 0.022 mM $Mg^{2+}$, n = 4.1, and a relative cleavage constant ratio ($k_u/k_f = 1\ t_{rel}^{-1}[Mg^{2+}]_{rel}^{-1}/0.2\ t_{rel}^{-1}[Mg^{2+}]_{rel}^{-1} = 5.0$). The folding RNA shifts between k = 1 and 0.2 $t_{rel}^{-1}[Mg^{2+}]_{rel}^{-1}$ trends (dashed and dotted lines) to form a Goldilocks zone. Goldilocks behavior requires conversion from folded to unfolded, slower cleavage of folded vs. unfolded RNA ($k_f < k_u$). (b) The simulated two-state reaction mechanism. U is unfolded RNA and F is folded RNA. (c) Effect of variation of $K_D$ while other parameters are held fixed. (d) Effect of variation of n. (e) Effect of variation of the cleavage rate constant of the folded RNA, $k_f$. (f) Effect of variation of the cleavage rate constant of the unfolded RNA, $k_u$. Each parameter was varied by multiplication or division by $1+(0.1\times2^i)$ (i = 1, 2, 3, …8). For this representation, $[Mg^{2+}]$ was

converted to $[Mg^{2+}]_{rel}$ where 1 $[Mg^{2+}]_{rel} = K_D = 0.022$ mM $Mg^{2+}$. Lifetime (t) was converted to $t_{rel}$ where $t_{rel} = 1$ when $[Mg^{2+}]_{rel} = 1$ and the cleavage constant(s) are always 1 $t_{rel}^{-1}[Mg^{2+}]_{rel}^{-1}$.

*Goldilocks behavior persists in complex models.* The simulations above assume two states (folded and unfolded), each associated with a cleavage rate constant. However, RNA folding often proceeds via one or more intermediate states (10). In a realistic folding mechanism, an intermediate might have a cleavage rate constant, $k_i$, that is different from those of the unfolded state ($k_u$) and the folded state ($k_f$). To model the contribution of folding intermediates to Goldilocks behavior, we modified **Eq. 4** using the approach of Shelton et al. (10) **(Supp. Eq. 1)**. The transition from unfolded to intermediate is described by the terms $K_{D1}$ and $n_1$, and the transition from intermediate to fully folded is described by $K_{D2}$ and $n_2$. We initialized the three-state equation in simulations using the parameter values and normalization method of **Figure 2**. Specifically, we set $K_{D1}$ at 1 $[Mg^{2+}]_{rel}$ and $k_u/k_f$ at 5. We set both $n_1$ and $n_2$ to 4.1 and $K_{D2}$ for the second transition to 2 $[Mg^{2+}]_{rel}$. $k_i$ was varied.

The simulations show that a three-state model can yield highly pronounced and robust Goldilocks zones **(Figure 3)**. When $k_i = k_f$ (black line), the intermediate is protected from cleavage, shifting the Goldilocks zone to lower $[Mg^{2+}]$ (zone 1). When $k_i < k_f$, the intensity of the Goldilocks zone increases at a $[Mg^{2+}]$ where the intermediate population is maximum. When $k_i = k_u$ (dotted line) only the folded state affords protection, giving a Goldilocks peak centered at a higher $[Mg^{2+}]$ (zone 2). Increasing the intermediate cleavage rate ($k_i > k_u$) deepens the valley at low $[Mg^{2+}]$ and accentuates peak 2. When $k_u < k_i < k_f$, the profile is intermediate between $k_i = k_f$ and $k_i = k_u$. Overall, RNAs with folding intermediates that either cleave more slowly than the fully folded state ($k_i < k_f$) or cleave more rapidly than the unfolded state ($k_i > k_u$) can occupy pronounced Goldilocks zones.

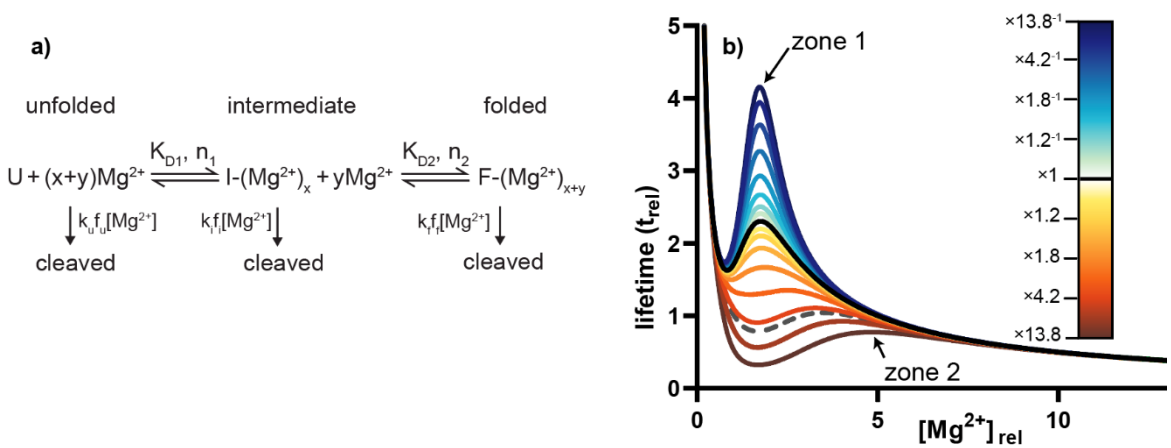


**Figure 3: Goldilocks behavior of RNA is observed with complex folding mechanisms.** (a) In a three-state mechanism, unfolded RNA converts in a first transition to an intermediate, which folds fully in a second transition. Unfolded RNA is cleaved with rate constant $k_u$, the intermediate is cleaved with rate constant $k_i$, and fully folded state is cleaved with rate constant of $k_f$. (b) In the simulation, $k_i$ was varied while other parameters were fixed ($k_u = 1$, $k_f = 0.2$, $K_{D1} = 1$ $[Mg^{2+}]_{rel}$, $n_1 = 4.1$, $K_{D2} = 2$ $[Mg^{2+}]_{rel}$ and $n_2 = 4.1$. The black line represents lifetimes when $k_i = k_f$. The dotted line represents a lifetimes when $k_i = k_u$. A $k_i < k_f$ scenario favors an early Goldilocks zone and a $k_i > k_u$ scenario favors a late Goldilocks zone.

*Experimental Characterization of Goldilocks behavior*. To experimentally investigate Goldilocks behavior, we assayed yeast $tRNA^{Phe}$ for rates of cleavage across a range of $[Mg^{2+}]$ **(Figure 4)**. Under the conditions of our experiment random coil yeast $tRNA^{Phe}$ folds to the L-shaped structure upon addition of $Mg^{2+}$ (28, 38-43). Multiple $Mg^{2+}$ ions coordinate the RNA in crystal structures (44) and in solution (45). We used yeast $tRNA^{Phe}$ because of cost, availability, and the wealth of previous information on structure and folding. We approximated native ionic strength, and elevated the temperature (65°C) to observe $Mg^{2+}$-dependent folding (46).

To determine the effect of $Mg^{2+}$ on extent of folding and on rate of cleavage, the tRNA was incubated at various $[Mg^{2+}]$ at constant temperature (65°C) and [NaCl] (180 mM) (**Figure 4**). Extent of folding was quantified by CD spectroscopy. As expected, a clear cooperative folding transition occurred with a midpoint at ~2 mM $Mg^{2+}$. Extent of cleavage was assayed at fixed times. Reaction mixtures were resolved by gel electrophoresis, and the amount of intact tRNA was quantified. This assay detects cleavage at any site, and therefore represents an average of cleavage rates over the tRNA. Band quantification revealed that at fixed time the fraction of intact (uncleaved) yeast $tRNA^{Phe}$ was greatest near 2.5 mM $Mg^{2+}$, where the tRNA is ~90% folded. The rate of tRNA cleavage is less at 2.5 mM $Mg^{2+}$ than at either 2.0 mM or at 3.5 mM $Mg^{2+}$. As a control, we used $rU_{20}$, which does not fold. $rU_{20}$ does not exhibit Goldilocks behavior.

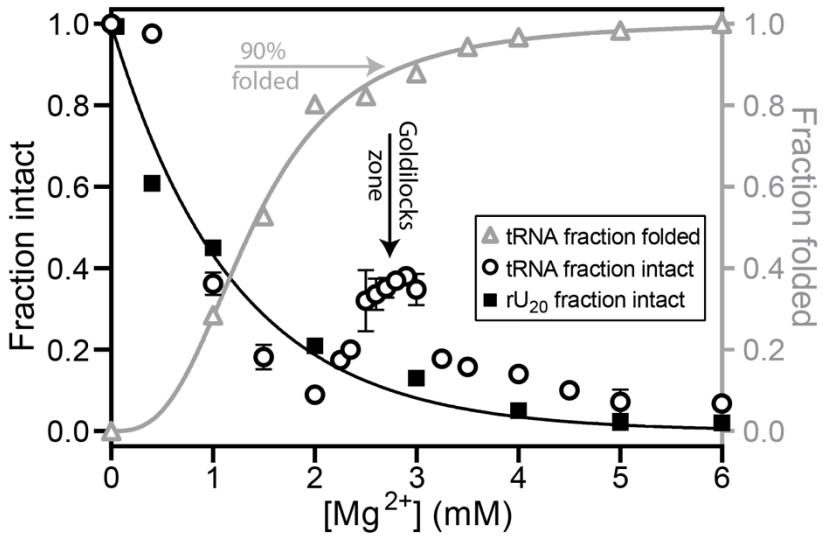


**Figure 4: Folding causes protection from cleavage**. The fraction cleaved of yeast $tRNA^{Phe}$ (open circles) and $rU_{20}$ (black squares) after 48 hours was determined by quantification of bands following PAGE. The fraction folded of yeast $tRNA^{Phe}$ (triangles) was determined by CD and was fit with the Hill equation. Extent of $rU_{20}$ cleavage (dashed line) was fit to a model with a single rate constant **(Supp. Eq. 2)**. $rU_{20}$ did not show a folding transition (not shown). Error bars represent the standard deviation of five replicates. Both CD and cleavage experiments were conducted in 180 mM NaCl, 50 mM HEPES pH 7.1 at 65°C, with variable $[Mg^{2+}]$.

The fraction of intact tRNA remaining at fixed time in **Figure 4** was converted to lifetime and fit by our models **(Figure 5)**. The model with two states reasonably predicts the observed Goldilocks zone. The calculated and observed Goldilocks zones are centered at the same $[Mg^{2+}]$. The cleavage

rate constant of the unfolded tRNA is predicted to be 2.5 times greater than that of the folded tRNA. However, the observed Goldilocks zone is more acute, with longer lifetimes, than predicted by the two-state model. A three-state folding model predicts a more acute Goldilocks zone, with greater relative protection. A three-state model fits the data more closely than the two-state model, especially in the center of the Goldilocks zone. In the three-state model the cleavage rate constant for the unfolded RNA is predicted to be 6.2 times that of the intermediate and 2.2 times that of the fully folded tRNA ($k_u > k_f > k_i$). The values of the parameters output by the fits are shown in **Table 1**. The significance of the better fit of the three-state versus the two-state model is indicated by the "Extra sum-of-squares F test" and inspection of residual errors **(Supp. Figure 2)**. The fundamental conclusion of this report, which is the prediction and confirmation of the Goldilocks zone, is not dependent on the model chosen to represent the system.

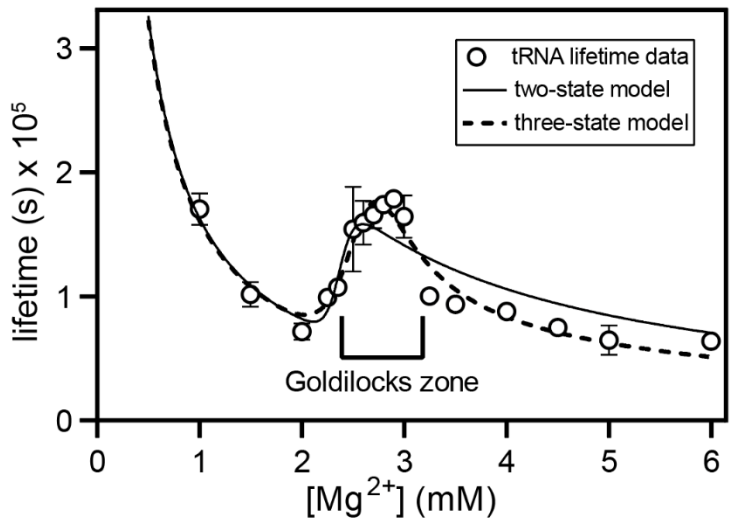


**Figure 5: tRNA lifetime shows a Goldilocks zone.** Yeast $tRNA^{Phe}$ lifetimes in solution are consistent with the simulations that predict a Goldilocks zone. The fraction of full-length tRNA after incubation for fixed time with variable [$Mg^{2+}$] (**Figure 4)** was converted to lifetime (black circles, error bars = std. dev; five replicates). The solid line is a fit with a two-state model and the dotted line is a fit with a three-state model. The data and both fits show a Goldilocks zone. The three-state model better approximates the data with a sharper spike in lifetime in the Goldilocks zone. The three-state model used an $n_2$ value of six for the intermediate to folded transition based on previous observations (33). All other parameters in our model were allowed to find their best fit values.

**Table 1: Parameters from fits to tRNA lifetime**

| | $k_u$ ($s^{-1}M^{-1}$) | $k_i$ ($s^{-1}M^{-1}$) | $k_f$ ($s^{-1}M^{-1}$) | $K_{D1}$ (mM) | $K_{D2}$ (mM) | $n_1$ | $n_2$ |
|---|---|---|---|---|---|---|---|
| Two-state | $6.1\times10^{-3}$ | -- | $2.4\times10^{-3}$ | 2.3 | -- | 33 | -- |
| Three-state | $6.2\times10^{-3}$ | $1.0\times10^{-3}$ | $2.8\times10^{-3}$ | 2.4 | 2.7 | 15 | 6* |

* $n_2$ fixed at 6, for the number of $Mg^{2+}$ binding sites (47) reported by Draper (33).

## Discussion

RNA can inhabit a "Goldilocks zone" of RNA protection flanked by conditions of fragility. The RNA Goldilocks phenomena appears to be robust and is maintained over a broad range of folding and cleavage parameters. Simulations predict that essentially any factor that modulates extent of folding will influence the characteristics of the Goldilocks zone but will not expunge it.

The center of the Goldilocks zone in relation to $[Mg^{2+}]$ is determined primarily by the affinity of folded RNA for $Mg^{2+}$ (which is related to the $K_D$). A smaller $K_D$ shifts the Goldilocks zone to lower $[Mg^{2+}]$. The ratio of cleavage rate constants of folded and unfolded states ($k_u/k_f$) is an important determinant of the shape of the Goldilocks zone. A pronounced Goldilocks zone occurs if $k_u/k_f > 2$ and the intensity of the Goldilocks zone increases with increasing $k_u/k_f$. When folding involves intermediate states, the Goldilocks zone is especially intense if the rate of cleavage of an intermediate state is less than those of the unfolded and folded states. The cooperativity of $Mg^{2+}$ binding, given by n, or the slope at the transition midpoint of the plot of fraction folded versus $[Mg^{2+}]$, is an important influence on the intensity of the zone. For tRNA under the conditions of our experiment, the binding transitions are sharp, taking place over a $\Delta[Mg^{2+}] = 2$ mM. This level of cooperativity is consistent with a pronounced Goldilocks zone. A Goldilocks zone is observed for folding mechanisms with or without intermediate states and can be more pronounced for RNAs with intermediate states. Important ancillary influences on the RNA Goldilocks zone would include monovalent cation concentrations, temperature, RNA sequence and chemical modification, and protein and ligand association. RNAs that do not fold cannot access a Goldilocks zone.

tRNA cleavage experiments confirm the predictions of the simulations. Yeast $tRNA^{Phe}$ inhabits a Goldilocks zone, with a local lifetime maximum near the $[Mg^{2+}]$ of near-complete folding. A two-state folding model, with two cleavage rate constants, predicts the general features of the experimentally observed Goldilocks zone for yeast $tRNA^{Phe}$. However, a three-state model provided significantly better fits to the observed intensity of the Goldilocks zone. The observed Goldilocks zone for the three-state model is more pronounced than predicted by the two-state model. A three-state model aligns with previous proposals for mechanisms of yeast $tRNA^{phe}$ folding (10, 28, 38, 48).

Our tRNA data are most consistent with a model in which the intermediate state has the lowest cleavage rate constant ($k_i < k_f < k_u$). Some previous reports suggest that yeast $tRNA^{Phe}$ is least compact when unfolded at low ionic strength, most compact at intermediate ionic strength, and moderately compact at high ionic strength (49-51). If so, the level of compaction might correlate with chemical lifetime (however, see reference (52)).

The Goldilocks concept should extend beyond $Mg^{2+}$ to species such as $Fe^{2+}$, which also promotes both RNA folding and cleavage (53, 54). Even farther, the general principles of a Goldilocks zone can be applied to any agent that has both a "positive" and "negative" effect on biopolymer lifetime. For example, protein folding requires aqueous media (55), yet, protein is cleaved by hydrolysis (56). Protein folding decreases rates of hydrolysis (1). Therefore, this model predicts a water-defined Goldilocks zone for proteins.

*The Goldilocks zone in vivo.* Our simulations predict that some RNAs *in vivo* inhabit a Goldilocks zone. Free $Mg^{2+}$ *in vivo* is near 1 mM (57, 58) **(Table S1**). As an example, it has been shown that a 58-nucleotide fragment of rRNA folds at around 1 mM $Mg^{2+}$ at *in vivo* ionic strength (150 mM

$K^+$) (59). The Goldilocks zone peak sits at the [$Mg^{2+}$] of near-maximal folding, meaning the Goldilocks zone and cellular $Mg^{2+}$ coincide at 1 mM. We expect this rRNA element is near the apex of its Goldilocks zone *in vivo*. The Goldilocks zone could explain in part why cells invest in careful maintenance of $Mg^{2+}$ homeostasis (60). It seems likely that a narrow range of [$Mg^{2+}$] prolongs specific RNA lifetimes *in vivo*.

The observation of Goldilocks behavior by RNA suggests a high level of sophistication of biopolymers. RNA is commonly described as fragile, but in fact is now seen to be subject to ultrafine control of chemical lifetime. Goldilocks behavior provides a mechanism of this control. RNA chemical lifetime can be tuned by shifts into and out of Goldilocks zones and by changing the profile of the zone.

*Origins of Life and the Goldilocks zone.* A Goldilocks zone may have played a role in the emergence of RNA during prebiotic chemical processes. It seems likely that rates of synthesis and degradation would have been selected during prebiotic chemical evolution (61). A state of finely controlled metastability, with access to a Goldilocks zone, could have been a natural outcome of chemical evolution. The conditions of the Goldilocks zones might point toward a historical metal concentration during the origins of life.

## Materials and Methods

*Reagents & Software.* Yeast $tRNA^{Phe}$ was purchased from Sigma-Aldrich (R4018). $rU_{20}$ was a custom oligo purchased from Integrated DNA Technologies. The software GraphPad Prism 8 was used for RNA lifetime simulations and for error analysis.

*Circular Dichroism*. A solution of 10 µM tRNA (strand) in 180 mM NaCl and 50 mM HEPES buffer pH 7.1 was added to a cuvette with a 1 cm path length. Spectra were accumulated on a Jasco J-810 spectrometer with scan rate of 200 nm/min, bandwidth of 3 nm, data pitch of 0.2 nm, from 200 to 320 nm at 65°C. The yeast $tRNA^{Phe}$ was titrated with small volumes of concentrated known $MgCl_2$ solutions. CD spectra were baseline-corrected and smoothed with a moving average. Fraction folded was estimated from the $theta_{max}$ at a given [$Mg^{2+}$] relative to the difference between the $theta_{max}$ of the fully folded and the unfolded tRNA. Fraction-folded data were fit with the Hill equation.

*In-line cleavage of RNA.* Solutions of 10 µM yeast $tRNA^{Phe}$ or $rU_{20}$ in 180 mM NaCl, 50 mM HEPES buffer pH 7.1, and 0.0, 1.0, 1.5, 2.0, 2.5, 3.0, 3.5, 4.0, 5.0, or 6.0 mM $MgCl_2$ were incubated at 65°C for 48 hours. Reaction mixtures were separated by electrophoresis on 7% urea PAGE gels run at 120V for 1 hour and stained with SYBR Green II. Stained gels were digitized with an Azure 6000 Imaging System (Azure Biosystems). Band intensities were quantified using AzureSpot Analysis software. $rU_{20}$ data were fit according to **Supp. Eqn. 2**. Yeast $tRNA^{Phe}$ data was converted to lifetime and fit to our lifetime models.

**Funding.** This work was supported by the National Aeronautics and Space Administration Astrobiology Program Center for the Origins of life 80NSSC18K1139.

**Acknowledgments.** We thank Drs. Jonathan B. Chaires Nicholas V. Hud, and Ramanarayanan Krishnamurthy for helpful discussions.

## References


1. Runnels CM, Lanier KA, Williams JK, Bowman JC, Petrov AS, Hud NV, & Williams LD (2018) Folding, Assembly, and Persistence: The Essential Nature and Origins of Biopolymers. *J Mol Evol* 86(9):598-610.
2. Regulski EE & Breaker RR (2008) In-Line Probing Analysis of Riboswitches. *Post-Transcriptional Gene Regulation*, ed Wilusz J (Humana Press, Totowa, NJ), pp 53-67.
3. Guth-Metzler R, Bray MS, Frenkel-Pinter M, Suttapitugsakul S, Montllor-Albalate C, Bowman JC, Wu R, Reddi AR, Okafor CD, & Glass JB (2020) Cutting In-line with Iron: Ribosomal Function and Non-Oxidative RNA Cleavage. *Nucleic Acids Res* 48(15):8663-8674.
4. Forconi M & Herschlag D (2009) Metal Ion-Based RNA Cleavage as a Structural Probe. *Methods Enzymol* 468:91-106.
5. Li Y & Breaker RR (1999) Kinetics of RNA Degradation by Specific Base Catalysis of Transesterification Involving the 2'-Hydroxyl Group. *J Am Chem Soc* 121(23):5364-5372.
6. Kuusela S & Lönnberg H (1993) Metal Ions That Promote the Hydrolysis of Nucleoside Phosphoesters Do Not Enhance Intramolecular Phosphate Migration. *J Phys Org Chem* 6(6):347-356.
7. Behlen LS, Sampson JR, Direnzo AB, & Uhlenbeck OC (1990) Lead-Catalyzed Cleavage of Yeast-$tRNA^{Phe}$ Mutants. *Biochemistry* 29(10):2515-2523.
8. Breslow R & Huang D-L (1991) Effects of Metal Ions, Including $Mg^{2+}$ and Lanthanides, on the Cleavage of Ribonucleotides and RNA Model Compounds. *Proc Natl Acad Sci USA* 88(10):4080-4083.
9. Bowman JC, Lenz TK, Hud NV, & Williams LD (2012) Cations in Charge: Magnesium Ions in RNA Folding and Catalysis. *Curr Opin Struct Biol* 22(3):262-272.
10. Shelton VM, Sosnick TR, & Pan T (2001) Altering the Intermediate in the Equilibrium Folding of Unmodified Yeast-$tRNA^{Phe}$ with Monovalent and Divalent Cations. *Biochemistry* 40(12):3629-3638.
11. Pan J, Thirumalai D, & Woodson SA (1999) Magnesium-Dependent Folding of Self-Splicing RNA: Exploring the Link between Cooperativity, Thermodynamics, and Kinetics. *Proc Natl Acad Sci USA* 96(11):6149.
12. Friederich MW & Hagerman PJ (1997) The Angle between the Anticodon and Aminoacyl Acceptor Stems of Yeast-$tRNA^{Phe}$ Is Strongly Modulated by Magnesium Ions. *Biochemistry* 36(20):6090-6099.
13. Sosnick TR (2001) Characterization of Tertiary Folding of RNA by Circular Dichroism and Urea. *Curr Protoc Nucleic Acid Chem* Chapter 11:Unit 11 15.
14. Cate JH, Hanna RL, & Doudna JA (1997) A Magnesium Ion Core at the Heart of a Ribozyme Domain. *Nat Struct Biol* 4(7):553-558.
15. Smith D & Pace NR (1993) Multiple Magnesium Ions in the Ribonuclease P Reaction Mechanism. *Biochemistry* 32(20):5273-5281.
16. Gesteland RF (1966) Unfolding of Escherichia Coli Ribosomes by Removal of Magnesium. *J Mol Biol* 18(2):356-IN314.
17. Sosunov V, Sosunova E, Mustaev A, Bass I, Nikiforov V, & Goldfarb A (2003) Unified Two-Metal Mechanism of RNA Synthesis and Degradation by RNA Polymerase. *EMBO J* 22(9):2234-2244.

18. Blaszczyk J, Tropea JE, Bubunenko M, Routzahn KM, Waugh DS, Court DL, & Ji X (2001) Crystallographic and Modeling Studies of RNase III Suggest a Mechanism for Double-Stranded RNA Cleavage. *Structure* 9(12):1225-1236.
19. Wacker WEC (1969) The Biochemistry of Magnesium. *Annals of the New York Academy of Sciences* 162(2):717-726.
20. Soukup GA & Breaker RR (1999) Relationship between Internucleotide Linkage Geometry and the Stability of RNA. *RNA* 5(10):1308-1325.
21. Ciesiołka J, Lorenz S, & Erdmann VA (1992) Structural Analysis of Three Prokaryotic 5S rRNA Species and Selected 5S rRNA--Ribosomal-Protein Complexes by Means of Pb(II)-Induced Hydrolysis. *Eur J Biochem* 204(2):575-581.
22. Nahvi A, Sudarsan N, Ebert MS, Zou X, Brown KL, & Breaker RR (2002) Genetic Control by a Metabolite Binding mRNA. *Chem Biol* 9(9):1043-1049.
23. Pan T (2000) Probing RNA Structure by Lead Cleavage. *Current Protocols in Nucleic Acid Chemistry* 00(1):6.3.1-6.3.9.
24. Ciesiołka J, Michałowski D, Wrzesinski J, Krajewski J, & Krzyżosiak WJ (1998) Patterns of Cleavages Induced by Lead Ions in Defined RNA Secondary Structure Motifs11edited by I. Tinoco. *J Mol Biol* 275(2):211-220.
25. Kaukinen U, Bielecki L, Mikkola S, Adamiak RW, & Lönnberg H (2001) The Cleavage of Phosphodiester Bonds within Small RNA Bulges in the Presence and Absence of Metal Ion Catalysts. *J Chem Soc Perk Trans 2* (7):1024-1031.
26. Barciszewska MZ, Perrigue PM, & Barciszewski J (2016) tRNA – the Golden Standard in Molecular Biology. *Molecular BioSystems* 12(1):12-17.
27. Kim SH, Suddath FL, Quigley GJ, Mcpherson A, Sussman JL, Wang AH, Seeman NC, & Rich A (1974) Three-Dimensional Tertiary Structure of Yeast Phenylalanine Transfer RNA. *Science* 185(4149):435-440.
28. Cole PE, Yang SK, & Crothers DM (1972) Conformational Changes of Transfer Ribonucleic Acid. Equilibrium Phase Diagrams. *Biochemistry* 11(23):4358-4368.
29. Sclavi B, Sullivan M, Chance MR, Brenowitz M, & Woodson SA (1998) RNA Folding at Millisecond Intervals by Synchrotron Hydroxyl Radical Footprinting. *Science* 279(5358):1940-1943.
30. Li PTX, Collin D, Smith SB, Bustamante C, & Tinoco I (2006) Probing the Mechanical Folding Kinetics of Tar RNA by Hopping, Force-Jump, and Force-Ramp Methods. *Biophys J* 90(1):250-260.
31. Hodak JH, Fiore JL, Nesbitt DJ, Downey CD, & Pardi A (2005) Docking Kinetics and Equilibrium of a GAAA Tetraloop-Receptor Motif Probed by Single-Molecule Fret. *Proc Natl Acad Sci USA* 102(30):10505.
32. Zarrinkar PP, Wang J, & Williamson JR (1996) Slow Folding Kinetics of RNase P RNA. *RNA (New York, NY)* 2(6):564-573.
33. Draper DE, Grilley D, & Soto AM (2005) Ions and RNA Folding. *Annu Rev Biophys Biomol Struct* 34(1):221-243.
34. Corbett JF (1972) Pseudo First-Order Kinetics. *J Chem Educ* 49(10):663.
35. El Seoud OA, Baader WJ, & Bastos EL (2016) Practical Chemical Kinetics in Solution. *Encyclopedia of Physical Organic Chemistry*:1-68.
36. Wayment-Steele HK, Kim DS, Choe CA, Nicol JJ, Wellington-Oguri R, Watkins AM, Sperberg RaP, Huang P-S, Participants E, & Das R (2020) Theoretical Basis for Stabilizing Messenger RNA through Secondary Structure Design. (Cold Spring Harbor Laboratory).

37. Rohatgi R, Bartel DP, & Szostak JW (1996) Nonenzymatic, Template-Directed Ligation of Oligoribonucleotides Is Highly Regioselective for the Formation of 3'−5' Phosphodiester Bonds. *J Am Chem Soc* 118(14):3340-3344.
38. Serebrov V, Clarke RJ, Gross HJ, & Kisselev L (2001) $Mg^{2+}$-Induced tRNA Folding. *Biochemistry* 40(22):6688-6698.
39. Friedrich K, Woolley P, & Steinhäuser KG (1988) Electrostatic Potential of Macromolecules Measured by pKa Shift of a Fluorophore. *Eur J Biochem* 173(1):233-239.
40. Thomas JC, Schurr JM, Reid BR, Ribeiro NS, & Hare D (1984) Effect of Magnesium(2+) on the Solution Conformation of Two Different Transfer Ribonucleic Acids. *Biochemistry* 23(23):5414-5420.
41. Robison B & Zimmerman TP (1971) A Conformational Study of Yeast Phenylalanine Transfer Ribonucleic Acid. *J Biol Chem* 246(1):110-117.
42. Maglott EJ, Deo SS, Przykorska A, & Glick GD (1998) Conformational Transitions of an Unmodified tRNA: Implications for RNA Folding. *Biochemistry* 37(46):16349-16359.
43. Privalov PL & Filimonov VV (1978) Thermodynamic Analysis of Transfer RNA Unfolding. *J Mol Biol* 122(4):447-464.
44. Shi H & Moore PB (2000) The Crystal Structure of Yeast Phenylalanine tRNA at 1.93 a Resolution: A Classic Structure Revisited. *RNA* 6(8):1091-1105.
45. Schauss J, Kundu A, Fingerhut BP, & Elsaesser T (2021) Magnesium Contact Ions Stabilize the Tertiary Structure of Transfer RNA: Electrostatics Mapped by Two-Dimensional Infrared Spectra and Theoretical Simulations. *J Phys Chem B* 125(3):740-747.
46. Blum AD, Uhlenbeck OC, & Tinoco I (1972) Circular Dichroism Study of Nine Species of Transfer Ribonucleic Acid. *Biochemistry* 11(17):3248-3256.
47. Leipply D & Draper DE (2010) Dependence of RNA Tertiary Structural Stability on $Mg^{2+}$ Concentration: Interpretation of the Hill Equation and Coefficient. *Biochemistry* 49(9):1843-1853.
48. Shelton VM, Sosnick TR, & Pan T (1999) Applicability of Urea in the Thermodynamic Analysis of Secondary and Tertiary RNA Folding. *Biochemistry* 38(51):16831-16839.
49. Olson T, Fournier MJ, Langley KH, & Ford NC (1976) Detection of a Major Conformational Change in Transfer Ribonucleic Acid by Laser Light Scattering. *J Mol Biol* 102(2):193-203.
50. Rhee KW, Potts RO, Wang C-C, Fournier MJ, & Ford NC, Jr. (1981) Effects of Magnesium and Ionic Strength on the Diffusion and Charge Properties of Several Single Trna Species. *Nucleic Acids Res* 9(10):2411-2420.
51. Fritzinger DC & Fournier MJ (1982) Chemical Modification Analysis of Ion-Dependent Changes in the Solution Structure of Yeast Phenylalanine tRNA. *Biochemistry* 21(9):2118-2127.
52. Fang X, Littrell K, Yang X-J, Henderson SJ, Siefert S, Thiyagarajan P, Pan T, & Sosnick TR (2000) $Mg^{2+}$-Dependent Compaction and Folding of Yeast-$tRNA^{Phe}$ and the Catalytic Domain of the B. Subtilis Rnase P RNA Determined by Small-Angle X-Ray Scattering. *Biochemistry* 39(36):11107-11113.
53. Athavale SS, Petrov AS, Hsiao C, Watkins D, Prickett CD, Gossett JJ, Lie L, Bowman JC, O'neill E, & Bernier CR (2012) RNA Folding and Catalysis Mediated by Iron (II). *PLoS One* 7(5):e38024.

54. Bray MS, Lenz TK, Haynes JW, Bowman JC, Petrov AS, Reddi AR, Hud NV, Williams LD, & Glass JB (2018) Multiple Prebiotic Metals Mediate Translation. *Proc Natl Acad Sci USA* 115(48):12164-12169.
55. Eisenberg D, Kauzmann W, & Kauzmann W (2005) *The Structure and Properties of Water* (Oxford University Press on Demand).
56. Radzicka A & Wolfenden R (1996) Rates of Uncatalyzed Peptide Bond Hydrolysis in Neutral Solution and the Transition State Affinities of Proteases. *J Am Chem Soc* 118(26):6105-6109.
57. Okorokov LA, Lichko LP, & Kulaev IS (1980) Vacuoles: Main Compartments of Potassium, Magnesium, and Phosphate Ions in *Saccharomyces Carlsbergenis* Cells. *J Bacteriol* 144(2):661-665.
58. Beeler T, Bruce K, & Dunn T (1997) Regulation of Cellular $Mg^{2+}$ by Saccharomyces Cerevisiae. *Biochim Biophys Acta* 1323(2):310-318.
59. Grilley D, Misra V, Caliskan G, & Draper DE (2007) Importance of Partially Unfolded Conformations for $Mg^{2+}$-Induced Folding of RNA Tertiary Structure: Structural Models and Free Energies of $Mg^{2+}$ Interactions. *Biochemistry* 46(36):10266-10278.
60. Romani AM (2011) Cellular Magnesium Homeostasis. *Arch Biochem Biophys* 512(1):1-23.
61. Frenkel-Pinter M, Haynes JW, Mohyeldin AM, Martin C, Sargon AB, Petrov AS, Krishnamurthy R, Hud NV, Williams LD, & Leman LJ (2020) Mutually Stabilizing Interactions between Proto-Peptides and RNA. *Nat Commun* 11(1):1-14.